Heat transfer characteristics of Taylor vortex flow with shear-thinning fluids

Masuda, Hayato
Shimoyamada, Makoto
Ohmura, Naoto

(Citation)
International Journal of Heat and Mass Transfer,130:274-281

(Issue Date)
2019-03

(Resource Type)
journal article

(Version)
Accepted Manuscript

Title:

Heat transfer characteristics of Taylor vortex flow with shear-thinning fluids

Authors:

Hayato Masuda[a,b,*], Makoto Shimoyamada[a], Naoto Ohmura[b,c]

Affiliation:

[a] School of Food and Nutritional Science, University of Shizuoka, 52-1 Yada, Suruga, Shizuoka 422-8526, Japan

[b] Complex Fluid and Thermal Engineering Research Center (COFTEC), Kobe University, 1-1 Rokkodai, Nada, Kobe 657-8501, Japan

[c] Department of Chemical Science and Engineering, Kobe University, 1-1 Rokkodai, Nada, Kobe 657-8501, Japan

Corresponding author:

* To whom correspondence should be addressed:

E-mail address: hayato-masuda@u-shizuoka-ken.ac.jp

Abstract

This study numerically investigates the heat transfer characteristics, including the fluid flow, of a Taylor vortex flow system with shear-thinning fluids. Governing equations were solved using OpenFOAM® 4.0 code. The Carreau model was utilized as the rheological model. The parameter (n) in the Carreau model, which describes the slope of a decrease in viscosity with an increase in shear-rate, was varied from 1 to 0.3. The local Nusselt number (Nu_L) decreased with the increase in shear-thinning property. Furthermore, a correlation equation between the effective Reynolds number (Re_{eff}) and a global Nusselt number (Nu_G) was proposed. Using this equation, Nu_G was evaluated within a ±10% error in the case of n = 1, 0.7, 0.5, and within a ±20% error in the case of n = 0.3. The size of the Taylor vortices became axially larger with an increase in the shear-thinning property. Furthermore, the thickness of the boundary layer of velocity and temperature increased with an increase in shear-thinning property. The ratio of the thickness of velocity boundary layer to the temperature boundary layer monotonically decreased with an increase in Re_{eff}.

Keywords: Taylor vortex flow, Heat transfer, Shear-thinning fluid, Nusselt number

1. Introduction

The flow between coaxial cylinders with the inner one rotating has been investigated from the various viewpoints since Taylor firstly reported its characteristics and complexity [1]. The flow regimes are characterized by circumferential Reynolds number (*Re*). When the *Re* exceeds a critical value (Re_{cr}), there appear pairs of counter-rotating toroidal vortices (Taylor vortices) regularly spaced along the axis, surrounding the inner cylinder like a vortex ring, as shown in Fig. 1. The toroidal motion of Taylor vortex flow enhances mixing within each Taylor vortex. In addition, all the fluid elements leaving the annulus have the same residence time when a relatively small axial flow is imposed in laminar vortex motion [2]. Since Kataoka et al. [2] reported these features of Taylor vortex flow, this flow system has been applied to various chemical processes, e.g., polymerization reaction [3], photocatalytic reaction [4], and decomposition of biopolymers [5]. In chemical processes, heating or cooling operation is often required. Thus, in order to apply a Taylor vortex flow system to such processes, Taylor vortex flow under a non-isothermal field is crucially important.

Many studies on the heat transfer characteristics of Taylor vortex flow with Newtonian fluids have been reported so far. From a practical viewpoint, the heat transfer coefficient must be adequately evaluated under the operational conditions. Based on theory or experiments, various equations correlating *Re* and the Nusselt number (*Nu*) were proposed in many papers [6–12]. Those correlation equations were reviewed by Fénot [13]. Both the heat transfer characteristics and the effect of buoyancy on the dynamics of Taylor vortex flow should be understood for the accurate design and control of processes. The effect of buoyancy on Taylor vortex flow with a radial heating or cooling has been investigated experimentally and numerically by several researchers [14–18]. They revealed that a series of various secondary flow regimes, induced by the classical Taylor vortices, were observed with an increase in the relative amount of buoyancy. Masuda et al. [19] investigated dynamics of Taylor vortex flow having the axial distribution of temperature. They classified it into three types of flow mode based on *Re* and the Grashof number (*Gr*), and showed the characteristics of mixing and heat transfer in each mode. Thus, although there are many studies about Taylor vortex flow under the non-isothermal field, they are limited to Newtonian fluid systems. From the practical viewpoint, studies conducted with non-Newtonian fluid systems are also important for chemical industries.

It is well known that the dynamics of Taylor vortex flow are significantly affected by non-Newtonian fluid properties, especially the elastic property. Muller et al. [20], Larson et al. [21], and Baumert and Muller [22] investigated the effect of elasticity on the flow dynamics experimentally and theoretically. They reported the original flow mode by the elastic instability. Wroński and Jastrzębski [23, 24] investigated the effect of the shear-thinning property on the stability experimentally and theoretically. Sinevic et al. [25] measured power number and torque for shear-thinning fluids experimentally. According to Escudier et al. [26], the structure of Taylor vortices is deformed by the shear-thinning property, and the vortex eye is shifted towards the surface of inner cylinder with an axial shift towards the radial outflow boundary. These previous studies focused on only the flow dynamics. There are few studies on the heat transfer characteristics with non-Newtonian fluids. To the author's best knowledge, a study by Naimi et al. [27] is one of the few studies of the heat transfer characteristics of Taylor vortex flow with shear-thinning fluids having yield stresses. Based on their experiments, they proposed the empirical correlation equation for the estimation of *Nu* under various flow regimes. However, the effect of viscosity distribution in the annular space caused by the shear-thinning property has not been assessed yet. After that, Khellaf and Lauriat [28] numerically investigated shear-thinning fluid dynamics and heat transfer in a Taylor vortex flow apparatus in detail. They concluded that the shear-thinning property decreases the friction factor at the rotating inner cylinder and enhances the heat transfer rate through the annular gap. Although they estimated the flow condition using Re_0 based on the zero shear-rate viscosity (η_0), the shear-thinning effect is not reflected in Re_0. It is inferred that the effective Re (Re_{eff}), which is defined based on the effective viscosity (η_{eff}) in the actual flow condition, is higher than Re_0 because the viscosity decreases due to the shear-thinning effect. Strictly speaking, the heat transfer performance in Newtonian fluid and shear-thinning fluid system is not accurately compared even under the same Re_0.

The objective of this study is (i) to investigate the effect of the shear-thinning property on the heat transfer characteristics based on Re_{eff} in which the shear-thinning effect is accurately reflected, and (ii) to propose a simple empirical correlation equation between Nu and Re_{eff} in shear-thinning fluid systems. How to define Re_{eff} is described in Section 3.1. For this purpose, it is necessary to reveal the local distributions of physical properties such as viscosity, velocity, and temperature, and compare them with those in Newtonian fluid systems. Here, computational fluid dynamics (CFD) is a powerful tool. If the governing equations are adequately solved, local information about physical properties can be obtained without insertion of some measurement probes that would disturb the flow field. In addition, the distribution of physical properties, which is difficult to measure experimentally, such as the local viscosity or shear-rate, is clarified easily. Therefore, numerical simulations were conducted to investigate fluid flow and heat transfer. For simplicity, it should be noted that there was no axial flow, and the flow condition was limited to the laminar Taylor vortex flow region.

2. Numerical simulation

2.1. Computational system

A computational domain consisted of concentric cylinders, a rotating inner cylinder (radius; R_i = 12.5 mm), and a fixed outer cylinder (radius; R_o = 17.5 mm), as shown in Fig. 2 (a) and (b). The gap width, d, and the radius ratio, R_i/R_o, were 5.0 mm and 0.71, respectively. Here, Re_{cr} is 82.2 when R_i/R_o = 0.71. The domain shown in Fig. 2 (a) was called "bounded system" because it was bounded by both side walls, and the length of cylinders, L, and aspect ratio, Γ, were 100 mm and 20, respectively. Furthermore, in order to investigate the end walls effect (Ekman boundary layer) on the heat transfer characteristics, the simulation with axially periodic boundary conditions ("no bounced system") was conducted, as shown in Fig. 2 (b). In this no bounded system, the length (L) and aspect ratio (Γ) were 10 mm and 2, respectively. The temperatures of the surfaces of the inner and outer cylinders were T_i and T_o, respectively. As the gravity force was parallel to the temperature gradient in this configuration, the effect of buoyancy on the flow was expected to be weak. For the boundary conditions of velocity, the circumferential velocity of the surface of inner cylinder was given as $u_\theta = R_i \times \omega$. Other walls were assumed to be fixed walls, i.e., $u_r = u_\theta = u_z = 0$. In the case of the no bounded system, the velocities of both side walls were set to be equal. With respect to the boundary conditions of pressure, there was no gradient at all walls. In order to assure the convergence regarding the conservation equation of energy, the small temperature difference between cylinders is preferable. Thus, T_i and T_o were set to 350.65 K and 355.65 K, respectively. The number of cells whose size is not uniform was 450,560 (32 × 64 × 220 in radial, circumferential, and axial directions, respectively) in the bounded system, and 45,056 (32 × 64 × 220) in the no bounded system, respectively. Cells were unequally spaced in the radial direction because finer resolution near walls was necessary owing to the steep velocity gradient. Fig. 3 (a) and (b) show the domain of bounded system at one cylinder and the whole picture, respectively. The number of cells was decided after checking their influence on the result (see Fig. 6).

2.2. Governing equations

The fluids used in the simulation were assumed to be incompressible shear-thinning fluids in a steady state. The problem should be made fully dimensionless in order to generalize the assessment of the flow and heat transfer performance. However, as de Souza Mendes pointed out [29], the non-dimensionalization of governing equations in non-Newtonian fluid systems is difficult. One of the reason is that how to choose the characteristic quantities, i.e. the deformation rate, has not been sufficiently discussed yet.

Thus, in this study, the non-dimensionalization was not conducted. In a three-dimensional simulation, the governing equations of fluid flow are conservation equations of mass, momentum, and energy, as shown in Eqs. (1) – (3):

$$\nabla \cdot \mathbf{u} = 0 \tag{1}$$

$$\frac{\partial \mathbf{u}}{\partial t} + (\mathbf{u} \cdot \nabla)\mathbf{u} = -\frac{\nabla p}{\rho} + \frac{1}{\rho}\nabla \cdot (2\eta\mathbf{D}) - \mathbf{g}\alpha(T - T_{\mathrm{ref}}) \tag{2}$$

$$\frac{\partial}{\partial t}\left(\rho C_{\mathrm{p}} T\right) + \nabla \cdot \left(\rho C_{\mathrm{p}} T \mathbf{u}\right) = \nabla \cdot (\kappa \nabla T) \tag{3}$$

where $\mathbf{u}$ is the velocity, t is the time, p is the pressure, ρ is the density, η is the viscosity, $\mathbf{D}$ (= $(\nabla\mathbf{u} + \nabla\mathbf{u}^{\mathrm{T}})/2$) is the deformation rate tensor, $\mathbf{g}$ is the gravitational acceleration, α is the coefficient of volume expansion, T is the temperature, T_{ref} is the reference temperature, C_{p} is the specific heat capacity, and κ is the thermal conductivity. In this study, $\partial\mathbf{u}/\partial t$ and $\partial(\rho C_{\mathrm{p}}T)/\partial t$ were neglected because the steady state was assumed. Here, the temperature change caused by viscous dissipation energy was neglected because the time scale assumed in this study was not so large. Nevertheless, it would be crucially important factor in highly viscous fluid systems. The simulation including the viscous dissipation energy term in Eq. (3) will be conducted in the future.

For shear-thinning fluids, the viscosity depends on the shear-rate. The shear-rate, $\dot{\gamma}$, is defined as $\dot{\gamma} = \sqrt{2D:D}$, which is the magnitude of the rate of deformation tensor. Here, the sign must be selected so that $\dot{\gamma}$ is a positive quantity. The rheological model that characterizes the relation between the viscosity and the shear-rate is required for the numerical simulation. In this study, the Carreau model, as shown in Eq. (4), was used because the transition to a constant viscosity at the limit of zero shear-rate is smooth:

$$\eta = \eta_0[1 + (\beta \cdot \dot{\gamma})^2]^{(n-1)/2} \tag{4}$$

where η_0 is the zero shear-rate viscosity, β is the characteristic time, and n is the power-law exponent.

In this simulation, the dependence of viscosity on the temperature was also included because many shear-thinning fluids are significantly varied even within the small temperature difference. The temperature dependence was expressed by an Arrhenius function:

$$\eta = \eta_{\mathrm{ref}} \exp\left[\frac{E}{R}\left(\frac{1}{T} - \frac{1}{T_{\mathrm{ref}}}\right)\right] \tag{5}$$

where E is the activation energy, and R is the gas constant. By combining Eqs. (4) and (5), the Carrau model equation with the temperature dependence was obtained as shown in Eq. (6):

$$\eta = (\eta_0)_{\mathrm{ref}}[1 + (\beta \cdot \dot{\gamma})^2]^{(n-1)/2} \exp\left[\frac{E}{R}\left(\frac{1}{T} - \frac{1}{T_{\mathrm{ref}}}\right)\right] \tag{6}$$

T_{ref} was set at 353.15 K (= $(T_{\mathrm{i}} + T_{\mathrm{o}})/2$). In this study, physical and rheological properties of a 1.0 wt% aqueous solution of hydroxyethlcellulose except n, in Eq. (6) was used [30]. Thus, the value of each of the parameters was as follows: ρ = 1003 kg/m^3, η_0 = 4.2 Pa·s,

β = 1.2 s, E = 26.1 kJ/mol, C_p = 3.71 kJ/kg·K, $\alpha = 3.30 \times 10^{-4}$ 1/K, κ = 0.534 W/m·K. n expresses the slope of decreasing viscosity in the power law region. In order to investigate the effect of the strength of the shear-thinning property on the heat transfer characteristics, the value of n was varied from 1 to 0.3. The rheological properties of fluids used in this study are shown in Fig. 4.

In order to solve the governing equations, OpenFOAM® 4.0 code was utilized. According to the previous simulation by the authors [31], the governing equations were discretized based on a finite volume method, and the second-order central difference scheme was applied to a convection and viscous term. The SIMPLE scheme was used for pressure-velocity coupling.

2.3. Validation of simulation code

For the purpose of validating the code, the results obtained by the simulation were compared with the experimental results by Kataoka [10]. The geometry of the computational system was the same as the experimental apparatus used in his study, i.e. R_i = 29 mm, R_o = 47 mm, L = 140 mm, and R_i/R_o = 0.62. It is noted that this geometry was used only for comparing the simulations and experiments. In this simulation, a Newtonian fluid was assumed. Re was set at 217.1 and 438.9. Here, Re_{cr} is 76.7 when

$R_i/R_o = 0.62$. Judging from Re/Re_{cr}, the flow regimes was inferred laminar Taylor vortex flow. The number of cells was $96 \times 64 \times 308$ in radial, circumferential, and axial directions, respectively. The axial variation in the local Nusselt number, Nu_L, at the surface of the outer cylinder was compared for simulations and experiments, as shown in Fig. 5. Here, the Nu_L was calculated from the gradient of the temperature at the outer cylinder surface, which was defined as

$$Nu_L = \frac{2hd}{\kappa} \tag{7}$$

where h is a local heat transfer coefficient, $h = q|_{r=R_o}/[(T_o - T_i)/2]$. In Fig. 5, it is noted that Nu_L was divided by the Prandtl number, Pr, to the one third. The axial position was normalized by half of the wavelength of a pair of Taylor vortices, $\lambda_{eff}/2$. As shown in Fig. 5, the comparison between the simulations and experiments showed good agreements. In addition, it was observed that Nu_L had a remarkable sinusoidal periodicity in the laminar Taylor vortex region. This is because the heat transfer coefficient in the laminar boundary layer around a circular cylinder in a cross-flow decreases with distance from the stagnation point and reaches a minimum in the neighborhood of the separation point [10]. Thus, Nu_L shows a maximum at the stagnation point of secondary flow (outflow boundary), and a minimum at the separation point (inflow boundary). It is noted that the purely hydrodynamic validation without heat transfer was already conducted in the previous work [31]. Moreover, the dependence of simulation results on the number of cells is shown in Fig. 6. It is noted that this check was conducted using the usual geometry of a computational system, i.e., R_i = 12.5 mm, R_o = 17.5 mm, L = 100 mm. A Newtonian fluid was assumed and Re was set at 109.0. The number of cells was 16 × 32 × 110 (system-1), 32 × 64 × 220 (system-2), and 48 × 96 × 330 (system-3), in radial, circumferential, and axial directions, respectively. Figure 5 shows the comparison of the axial distribution of Nu_L between each system. There was no significant difference in system-2 and system-3. Thus, 32 × 64 × 220 (system-2) was selected in order to reduce the calculation time.

3. Results and discussion

3.1. Effect of shear-thinning property on heat transfer characteristics

Figure 7 shows the effect of boundary conditions on a global Nusselt number, Nu_G, in Newtonian fluid systems. Nu_G was calculated as follows:

$$Nu_G = \int_0^L Nu_L dz \quad (8)$$

In the case of $Re \leq 200$, Nu_G in the bounded system was higher than it in the no bounded system due to the enhancement of heat transfer at Ekman boundary layers. On the other hand, $Re \geq 240$, the order was changed. This tendency agreed with the one reported by

Lopez et al. [32]. As shown in Fig. 7, it is considered that the effect of boundary conditions at side walls on the heat transfer performance is not negligible. The no bounded system is significantly effective for the reduction of computational cost, especially in the case of large temperature differences between T_i and T_o. As Lopez et al. [32] pointed out, only a short central fraction of the apparatus needs to be simulated to estimate transport properties. However, even the structure of Taylor vortices around the central fraction of the apparatus, which somewhat affects the local fluid flow and heat transfer, is affected by Ekman boundary layers [33, 34]. Furthermore, according to Kuo and Ball [15], the flow filed drastically changes due to Ekman cells if the buoyancy becomes stronger. Although the buoyancy was assumed to be small in this study, the simulation with the bounded system for the case of stronger buoyancy would be unavoidable in the future. In addition, from the practical viewpoint, the performance in the bounded system should be investigated because actual apparatuses have the finite length. Thus, the bounded system including the effect of Ekman boundary layers was selected for the investigation about the heat transfer performance in shear-thinning fluid systems.

For shear-thinning fluid systems, the approach used to define *Re* should first be discussed because viscosity spatially varies in the annular space. As Ohta et al. [35] pointed out, *Re* based on the zero shear-rate viscosity (η_0) underpredicts the true value for shear-thinning fluid systems. From a practical viewpoint, the definition of effective Re (Re_{eff}) is crucially important. In other words, appropriately defining the effective viscosity, η_{eff}, is the key to defining Re_{eff}. Thus, in order to define Re_{eff} from η_{eff}, it is necessary to properly estimate the effective shear-rate, $\dot{\gamma}_{\mathrm{eff}}$. Masuda et al. [31] proposed an empirical correlation equation for the rotational speed of the inner cylinder (ω) and the effective shear-rate ($\dot{\gamma}_{\mathrm{eff}}$) as follows:

$$\dot{\gamma}_{\mathrm{eff}} = \left\{77.05n^{0.32}\left(\frac{R_{\mathrm{i}}}{R_{\mathrm{o}}}\right)^2 - 88.73n^{0.31}\left(\frac{R_{\mathrm{i}}}{R_{\mathrm{o}}}\right) + 26.85n^{0.21}\right\} \cdot \omega \qquad (9)$$

where n is the rheological parameter in the Carreau model. If n and ω are introduced into Eq. (8), $\dot{\gamma}_{\mathrm{eff}}$ is calculated. After that, η_{eff} and Re_{eff} can be calculated easily, in turn. The critical Re_{eff}, at which Taylor vortices fully develop in the annular space, is in agreement with the Re_{cr} obtained from the linear stability analysis for Newtonian fluids. Therefore, Re_{eff} is applicable as a practical basis.

Figure 8 shows the axial variation in Nu_{L} at $Re_{\mathrm{eff}} = 158$. It is noted that z / ($\lambda_{\mathrm{eff}}/2$) = 0, 2 corresponds to the inflow boundaries, and z / ($\lambda_{\mathrm{eff}}/2$) = 1 correspond to the outflow boundary. As clearly shown in Fig. 8, Nu_{L} decreased with an increase in the shear-thinning property. It is considered that the viscosity distribution generated by the shear-thinning property decreases the fluidity. As a result, the heat transfer coefficient, i.e. Nu_{L}, decreased. The discussion based on Re_{eff} allowed to understand the intrinsic effect of the shear-thinning property on the heat transfer performance. In shear-thinning fluid systems, the viscosity distribution in the annular space at Re_{eff} = 158 is show in Fig. 9. The local viscosity was normalized by the effective viscosity (η_{eff}). It can be seen that the viscosity near the surface of the inner cylinder decreases due to the shear caused by the rotation of the inner cylinder. Furthermore, the viscosity decreased where the outflow impinged on the outer cylinder, i.e., the stagnation point. On the other hand, the viscosity near the separation point is relatively higher than that in other regions. As clearly shown in Fig. 9, the region where the viscosity is higher or lower than η_{eff} increased with an increase in the shear-thinning property. This means that, in highly shear-thinning fluid systems like n = 0.3, it is significantly difficult to describe the characteristics of fluid flow and heat transfer using one representative physical property, e.g., η_{eff}. Nevertheless, from a practical viewpoint, correlation equation for Re and Nu should be established.

According to Aoki et al. [9], Nu_{G} is theoretically expressed as follows:

$$Nu_{\mathrm{G}} = \left[1 + 1.438\left\{1 - \left(\frac{Re_{\mathrm{cr}}}{Re}\right)^2\right\}\right] \cdot \frac{\delta}{\delta_{\mathrm{t}}} \tag{10}$$

where δ is the velocity boundary layer thickness, and δ_{t} is the temperature boundary layer thickness. In the case of heat transfer under the forced convection of flat plates, the well-known relation holds:

$$\frac{\delta}{\delta_t} \cong Pr^{1/3} \tag{11}$$

Strictly speaking, although single flat plate analysis is not adequate to represent the interaction between the velocity and temperature boundary layers, Aoki et al. [9] successfully proposed the correlation equation combining Eqs. (10) and (11). Tachibana et al. [36] expressed the ratio of the velocity boundary layer thickness to the temperature boundary layer thickness as $Pr^{1/4}$. Figure 10 shows the relation between $Nu_{\mathrm{G}}/Pr_{\mathrm{eff}}^{m}$ and Re_{eff} in Newtonian fluids and various shear-thinning fluids. Here, $Pr_{\mathrm{eff}} = \eta_{\mathrm{eff}} C_{\mathrm{p}}/\kappa$ in shear-thinning fluid systems. It should be noted that the exponent of Pr_{eff}, m, was 1/3 for $n = 1$, 0.7, 0.5, and 1/3.6 for $n = 0.3$. This difference in the value of m means that the interaction between the velocity and temperature boundary layers would be affected by the high shear-thinning property in the case of $n = 0.3$. Moreover, the fitting line expressed by Eq. (12) was drawn in Fig. 10.

$$\frac{Nu_{\mathrm{G}}}{Pr_{\mathrm{eff}}^{m}} = 3.4 + 6.2\left\{1 - \left(\frac{Re_{\mathrm{cr}}}{Re}\right)^{2}\right\} \qquad (12)$$

The different constants in Eqs. (10) and (12) would be explained by the difference in Pr. Equation (10) was theoretically derived based on the assumption that $Pr \cong 1$ [8]. As shown in Fig. 10, using Eq. (12), Nu_{G} can be estimated within a ±10% error in the case of $n = 1$, 0.7, 0.5, and within a ±20% error in the case of $n = 0.3$. Thus, the practically useful correlation equation for process design and control was established. In the future, from the practical viewpoint, the heat transfer characteristics at higher Re_{eff} should be investigated. However, the investigation is not easy because the flow transition with an increase in Re_{eff} remains unclear until now. Recently, Alibenyahia et al. [37] and Cagney and Balabani [38] have investigated flow transitions with shear-thinning fluids theoretically and experimentally. Further investigations about flow transitions with higher instabilities is expected.

3.2. Effect of shear-thinning property on local characteristics of Taylor vortices

The effect of the shear-thinning property on characteristics such as the local fluid flow and the local heat transfer is important from a practical and scientific viewpoint. For Taylor vortex flow system, the structure of Taylor vortices influences the local heat transfer, mass transfer, and mixing. Because these local characteristics influence the global performance of the apparatus, the structure of Taylor vortices should be understood. Figure 11 shows the variation in the number of pairs of Taylor vortices, N, with Re_{eff}. In all cases, N tended to increase with an increase in Re_{eff} though some increases or decreases were observed. In other words, the size of the Taylor vortices decreases with an increase in Re_{eff}. This observation agrees with the simulations reported in several studies [33, 34]. It is noted that these studies were conducted under the isothermal field. In fact, precise control of the structure of Taylor vortices is difficult because the Taylor vortex flow system has multiplicities that are characterized by the hysteresis, the start-up operation, and physical properties of the fluid [39]. According to Coles [40], there are 26 stable states at a single *Re*. Furthermore, Mullin [41] and Benjamin and Mullin [39] experimentally obtained at least 39 steady flows.

In particular, it is well known that the number of pairs of Taylor vortices is significantly affected by how the flow condition reaches the steady state. For example, Ohmura et al. [42] varied the number of pairs of Taylor vortices by accurately controlling the acceleration of the inner cylinder using the computer-aided controller. Nevertheless, three types of stable states were probabilistically observed. This means that the perfect control of the number of pairs of Taylor vortices would be impossible. Furthermore, the number of pairs of Taylor vortices at the steady state is affected by how Ekman cells develop after the rotation of the inner cylinder [35]. In this study, the hysteresis and transient process was not taken into consideration because of the steady state simulation. The unsteady state simulation for the observation of development process of Taylor vortices requires a lot of calculation time. Thus, a precise discussion of the bifurcation process with an increase in Re or Re_{eff} is not conducted. Nevertheless, as clearly shown in Fig. 11, N decreased with an increase in the shear-thinning property at the same degree of Re_{eff}. It is considered that the shear-thinning property makes Taylor vortices axially large. Because the aspect ratio, $\Gamma(= L/d)$, was 20 in the bounded system, axially stretched Taylor vortices whose wavelength is larger than 2 were formed when $N < 10$. In shear-thinning fluid systems, such stretched Taylor vortices are often observed. For example, in the case of $n = 0.3$, N was below 10 except $Re_{\mathrm{eff}} = 158$. According to Watanabe et al. [43] and Norouzi et al. [44], Taylor vortices was axially stretched in viscoelastic fluid systems. It is noted that the elastic property was not assumed in this simulation. Based on the fact that the axially stretched Taylor vortices were observed in shear-thinning fluid systems without an elastic property, the elasticity and the shear-thinning property play an important role in the deformation of Taylor vortices. In order to clarify the effect of the shear-thinning property on the structure of Taylor vortices in more detail, the dynamic process of formation of Taylor vortices after the start of the rotation of the inner cylinder, including the viscosity distribution, should be numerically and experimentally investigated in the future.

Information about the local heat transfer characteristics is also obtained from simulation results. The Taylor cell adjacent to the end wall is significantly affected by Ekman pumping. Therefore, in order to investigate the local heat transfer in a Taylor vortex flow system, Taylor vortices around the middle of the apparatus are preferable for the elimination of the effect of the Ekman layer on local transport phenomena. From a local viewpoint, the outflow that is discharged from the inner cylinder impinged at the outer cylinder, and then, the local heat transfer was promoted at the stagnation point. Thus, to clarify the local heat transfer characteristics, including the fluid flow on the outflow, it is quite necessary to understand the local heat transfer characteristics in a Taylor cell. Figure 12 shows the radial distribution for (a) the circumferential velocity and (b) temperature on the outflow boundary at $Re_{\mathrm{eff}} = 158$. Both the circumferential velocity and temperature were normalized. It is noted that the outflow between Taylor vortices around the middle of the apparatus was selected. Figure 12 (a) shows the shear-thinning property has a damping effect on the velocity. This means that the viscosity distribution caused by the shear-thinning property has a negative effect on fluidity. The velocity distribution in this condition, $Re_{\mathrm{eff}} = 158$, became roughly flat in the center of the gap owing to the mixing motion by the Taylor vortices. In this study, according to Aoki et al. [9], the dimensionless thickness of the velocity boundary layer at the surface of the outer cylinder on the outflow, δ/d, is assumed as shown in Fig. 12 (a). As shown in Fig. 12 (a), the velocity boundary layer thickness increased with an increase in the shear-thinning property. Figure 12 (b) clearly shows that the temperature distribution was significantly affected by the damping effect on the velocity in shear-thinning fluid systems. The bulk temperature decreased with an increase in the shear-thinning property. Moreover, as shown in Fig. 12 (b), the dimensionless thickness of the temperature boundary layer at the surface of the outer cylinder on the outflow, δ_t/d, increased with an increase in the shear-thinning property. It was found that the shear-thinning property increases both the thicknesses of the velocity and temperature boundary layers. Figure 13 shows the dependence of the dimensionless thickness of (a) velocity boundary layer and (b) temperature boundary layer on Re_{eff} at the surface of the outer cylinder on the outflow. As shown in Figs. 13 (a) and (b), both thicknesses exponentially decreased with an increase in Re_{eff}. The degree of decrease clearly became more intense with an increase in the shear-thinning property. It was found that both thicknesses approached a constant. In all cases, except n = 0.3, the constants were approximately close in value. This means that the process of development of the boundary layer differs in the highly shear-thinning fluid system. Both the boundary layer thickness and ratio of the velocity boundary layer thickness to the temperature boundary layer thickness are important when studying heat transfer performance, as shown in Eq. (10). Based on Fig. 13, the dependence of the ratio, δ/δ_t on Re_{eff} was calculated as shown in Fig. 14. The line of $Pr_{\mathrm{eff}}^{\mathrm{m}}$ was also drawn in Fig. 14. The value of m is 1/3 for n = 1, 0.7, 0.5, and 1/3.6 for n = 0.3, respectively. In shear-thinning fluid systems, δ/δ_t monotonically decreased with an increase in Re_{ff}. As clearly shown in Fig. 14, the ratio roughly corresponded to Pr_{eff}^{m} although some deviations from

Pr_{eff}^{m} were observed in the case of $n = 0.3$. Thus, the value of m proposed in this study (Eq. (12)) seems to be rational. In the future, determining the dependence of m on the rheological properties of fluids would be necessary for the improvement of the accuracy of the proposed correlation equation.

4. Conclusions

This study numerically investigated the heat transfer characteristics of Taylor vortex flow with shear-thinning fluids. By changing the value of parameter, n, in the Carreau model, various types of shear-thinning fluids were used for the simulation. A local Nusselt number (Nu_{L}) decreased with an increase in the shear-thinning property. It is considered that the viscosity distribution generated by the shear-thinning property decreases the fluidity. In addition, a correlation equation between the effective Reynolds number (Re_{eff}) and a global Nusselt number (Nu_{G}) was proposed. Using this equation, Nu_{G} was evaluated within a ±10% error in the case of $n = 1, 0.7, 0.5$, and within a ±20% error in the case of $n = 0.3$.

It was found that the shear-thinning property makes Taylor vortices axially large. Furthermore, the shear-thinning property increases the thicknesses of the velocity and temperature boundary layers. In the future, the interaction between the velocity and temperature boundary layers should be investigated in a wide region of Re_{eff} and various type of non-Newtonian fluids. In addition, simulations in the large temperature gradient (beyond Boussinesq approximation), and higher Re_{eff} region (e. g. wavy Taylor vortex flow region) will be conducted for further understanding of heat transfer characteristics of Taylor vortex flow with shear-thinning fluids.

Acknowledgement

This research was financially supported by the Urakami Foundation for Food and Food Culture Promotion and JSPS KAKENHI Grant Number JP18H03853.

References

[1] G. I. Taylor, Stability of a viscous liquid contained between two rotating cylinders, Philos. Trans. R. Soc. A. 223 (1923) 289–343.

[2] K. Kataoka, H. Doi, T. Hongo, M. Futagawa, Ideal plug-flow properties of Taylor vortex flow, J. Chem. Eng. Japan 8 (1975) 472–476.

[3] K. Kataoka, N. Ohmura, M. Kouzu, Y. Simamura, M. Okubo, Emulsion polymerization of styrene in a continuous Taylor vortex flow reactor, Chem. Eng. Sci. 50(9) (1995) 1409–1416.

[4] J. G. Sczechowski, C. A. Koval, R. D. Noble, A Taylor vortex reactor for heterogeneous photocatalysis, Chem. Eng. Sci. 50(20) (1995) 3163–3173.

[5] H. Masuda, T. Horie, R. Hubacz, N. Ohmura, Process intensification of continuous starch hydrolysis with a Couette–Taylor flow reactor, Chem. Eng. Res. Des. 91(11) (2013) 2259–2264.

[6] I. S. Bjorklund, W. M. Kays, Heat transfer between concentric rotating cylinders, J. Heat Transfer 81 (1959) 175–186.

[7] K. M. Becker, J. Kaye, Measurements of diabatic flow in an annulus with an inner rotating cylinder, J. Heat Transfer 84 (1962) 97–105.

[8] C. Y. Ho, J. L. Nardacci, A. H. Nissan, Heat transfer characteristics of fluids moving

in a Taylor system of vortices, AIChE J. 10(2) (1964) 194−202.

[9] H. Aoki, H. Nohira, H. Arai, Convective heat transfer in an annulus with an inner rotating cylinder, Bull. JSME 10(39) (1967) 523−532.

[10] K. Kataoka, Heat-transfer in a Taylor vortex flow, J. Chem. Eng. Japan 8(4) (1975) 271−276.

[11] K. Kataoka, H. Doi, T. Komai, Heat/mass transfer in Taylor vortex flow with constant axial flow rates, Int. J. Heat Mass Transfer 20 (1977) 57−63.

[12] S. Poncet, S. Haddadi, S. Viazzo, Numerical modeling of fluid flow and heat transfer in a narrow Taylor−Couette−Poiseuille system, Int. J. Heat Fluid Flow 32 (2011) 128−144.

[13] M. Fénot, Y. Bertin, E. Dorignac, G. Lalizel, A review of heat transfer between concentric rotating cylinders with or without axial flow, Int. J. Therm. Sci. 50 (2011) 1138−1155.

[14] K. S. Ball, B. Farouk, V. C. Dixit, An experimental study of heat transfer in a vertical annulus with a rotating inner cylinder, Int. J. Heat Mass Transfer 32(8) (1989) 1517−1527.

[15] D. –C. Kuo, K. S. Ball, Taylor−Couette flow with buoyancy: onset of spiral flow, Phys. Fluids 9(10) (1997) 2872−2884.

[16] R. Kedia, M. L. Hunt, T. Colonius, Numerical simulations of heat transfer in Taylor−Couette flow, J. Heat Transfer 120 (1998) 65−71.

[17] R. Guillerm, C. Kang, C. Savaro, V. Lepiller, A. Prigent, K. –S. Yang, I. Mutabazi, Flow regimes in a vertical Taylor−Couette system with a radial thermal gradient, Phys. Fluids 27 (2015) 094101.

[18] H. Teng, N. Liu, X. Lu, B. Khomami, Direct numerical simulation of Taylor-Couette flow subjected to a radial temperature gradient, Phys. Fluids 27 (2015) 125101.

[19] H. Masuda, S. Yoshida, T. Horie, N. Ohmura, M. Shimoyamada, Flow dynamics in Taylor−Couette flow reactor with axial distribution of temperature, AIChE J. 64(3) (2018) 1075−1082.

[20] S. J. Muller, R. G. Larson, E. S. G. Shaqfeh, A purely elastic transition in Taylor-Couette flow, Rheol. Acta, 28 (1989) 499−503.

[21] R. G. Larson, E. S. G. Shaqfeh, S. J. Muller, A purely elastic instability in Taylor−Couette flow, J. Fluid Mech. 218 (1990) 573−600.

[22] B. M. Baumert, S. J. Muller, Flow visualization of the elastic Taylor-Couette instability in Boger fluids, Rheol. Acta 34 (1995) 147−159.

[23] S. Wroński, M. Jastrzębski, Experimental investigations of the stability limit of the helical flow of pseudoplastic liquids, Rheol. Acta 29 (1990) 453−461.

[24] S. Wroński, M. Jastrzębski, The stability of the helical flow of pseudoplastic liquids in a narrow annular gap with a rotating inner cylinder, Rheol. Acta 29 (1990) 442−452.

[25] V. Sinevic, R. Kuboi, A. W. Nienow, Power numbers, Taylor numbers and Taylor vortices in viscous Newtonian and non-Newtonian fluids, Chem. Eng. Sci. 41(11) (1986) 2915−2923.

[26] M. P. Escudier, I. W. Gouldson, D. M. Jones, Taylor vortices in Newtonian and shear-thinning liquids, Proc. Roy. Soc. Lond. A 449 (1995) 155−176.

[27] M. Naimi, R. Devienne, M. Lebouche, Etude dynamique et thermique de l'écoulement de Couette−Taylor−Poiseuille; cas d'un fluide présentant un seuil d'écoulement, Int. J. Heat Mass Trasfer 33 (2) (1990) 381−391.

[28] K. Khellaf, G. Lauriat, Numerical study of heat transfer in a non-Newtonian Carreau-fluid between rotating concentric vertical cylinders, J. Non-Newtonian Fluid Mech. 89 (2000) 45−61.

[29] P. R. de Souza Mendes, Dimensionless non-Newtonian fluid mechanics, J. Non-Newtonian Fluid Mech. 147 (2007) 109−116.

[30] M. Kaminoyama, M. Watanabe, K. Nishi, M. Kamiwano, Numerical simulation of local heat transfer coefficients in stirred vessel with impeller for highly viscous fluids, J. Chem. Eng. Japan 32(1) (1999) 23−30.

[31] H. Masuda, T. Horie, R. Hubacz, M. Ohta, N. Ohmura, Prediction of onset of Taylor−Couette instability for shear-thinning fluids, Rheol. Acta 56 (2017) 73−84.

[32] J. M. Lopez, F. Marques, M. Avila, Conductive and convective heat transfer in fluid flows between differentially heated and rotating cylinders, Int. J. Heat Mass Transfer 90 (2015) 959–967.

[33] J. E. Burkhalter, E. L. Koschmieder, Steady supercritical Taylor vortices after sudden starts, Phys. Fluids 174(11) (1974) 1929–1935.

[34] G. P. Neitzel, Numerical computation of time-dependent Taylor-vortex flows in finite-length geometries, J. Fluid Mech. 141 (1984) 51–66.

[35] M. Ohta, E. Iwasaki, E. Obata, Y. Yoshida, Dynamic processes in a deformed drop rising through shear-thinning fluids, J. Non-Newtonian Fluid Mech. 132 (2005) 100–107.

[36] F. Tachibana, S. Fukui, H. Mitsumura, Heat transfer in an annulus with an inner rotating cylinder, Trans. Jap. Soc. Mech. Engrs. 25(156) (1959) 788–792.

[37] B. Alibenyahia, C. Lemaitre, C. Nouar, N. Ait-Messaoudene, Revisiting the stability of circular Couette flow of shear-thinning fluids, J. Non-Newtonian Fluid Mech. 183–184 (2012) 37–51.

[38] N. Cagney, S. Balabani, Influence of shear-thinning on the mixing dynamics in a Taylor-Couette reactor, Proceedings of European Conference on Mixing, Toulouse, France, September 9th–12th, 2018

[39] T. B. Benjamin, T. Mullin, Notes on the multiplicity of flows in the Taylor experiment,

J. Fluid Mech. 121 (1982) 219–230.

[40] D. Coles, Transition in circular Couette flow, J. Fluid Mech. 21 (1965) 385–425.

[41] T. Mullin, Murations of steady cellular flows in the Taylor experiments, J. Fluid Mech. 121 (1982) 207–218.

[42] N. Ohmura, T. Makino, A. Motomura, Y. Shibata, K. Kataoka, Int. J. Heat Fluid Flow 19 (1998) 159–166.

[43] K. Watanabe, S. Sumio, S. Ogata, Formation of Taylor vortex flow of polymer solutions, J. Fluids Eng. 128 (2006) 95–100.

[44] M. Norouzi, A. Jafari, M. Mahmoudi, A numerical study on nonlinear dynamics of three-dimensional time-depended viscoelastic Taylor-Couette flow, Rheol. Acta 57 (2018) 127–140.

Figures

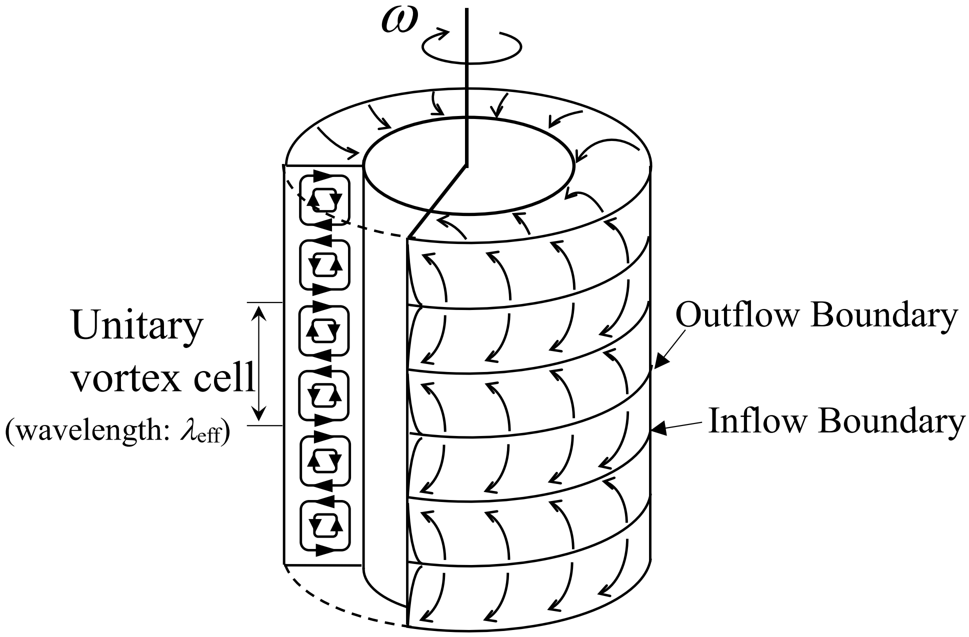

Figure 1 Taylor vortex flow

(a)

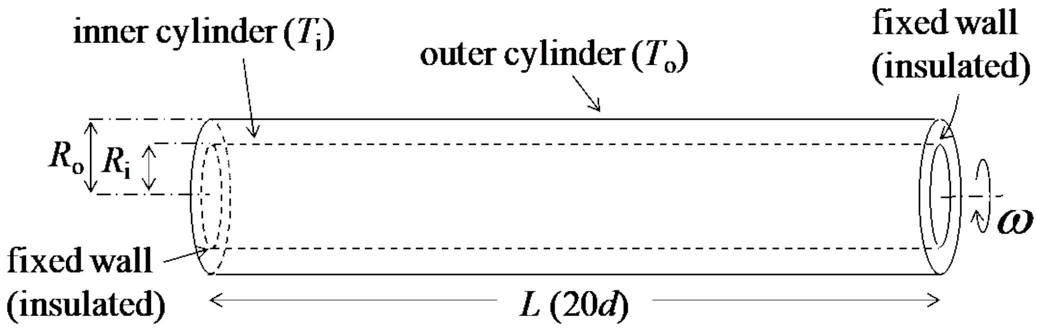

(b)

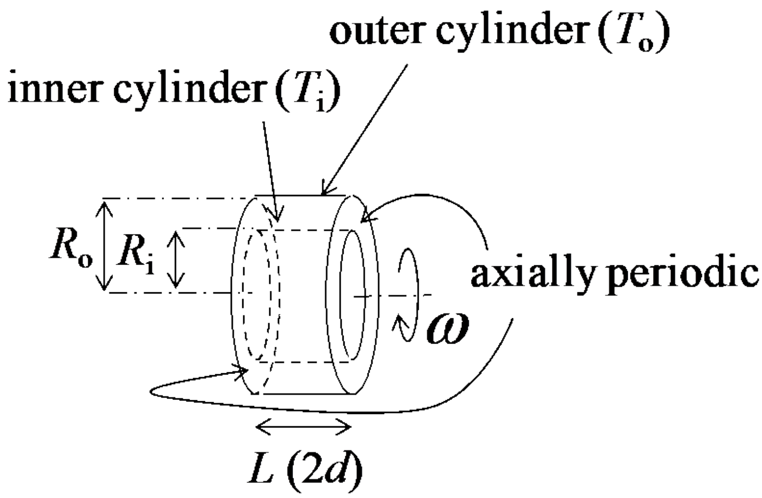

Figure 2 Computational domain and boundary conditions; (a) bounded system, (b) no bounded system (axially periodic boundary conditions).

(a)

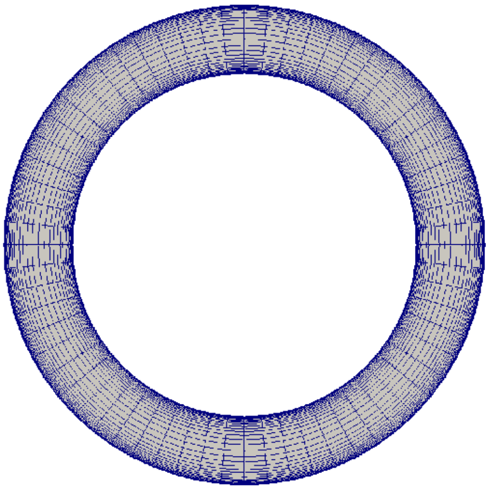

(b)

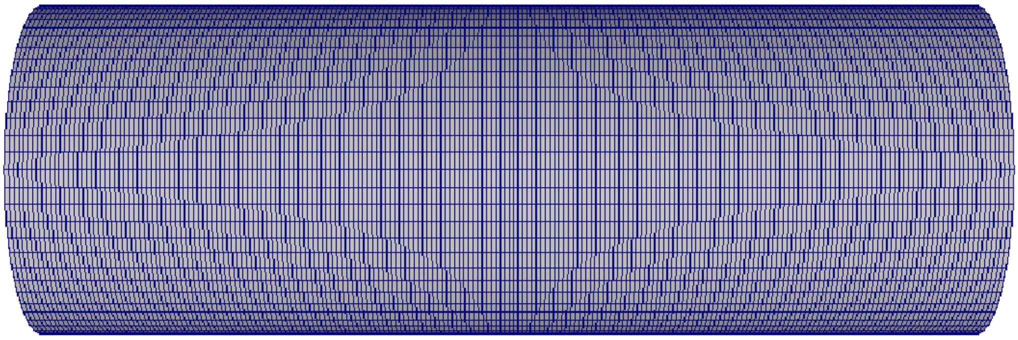

Figure 3 Computational domain with structured meshes; (a) cylinder cross-section, (b) whole picture

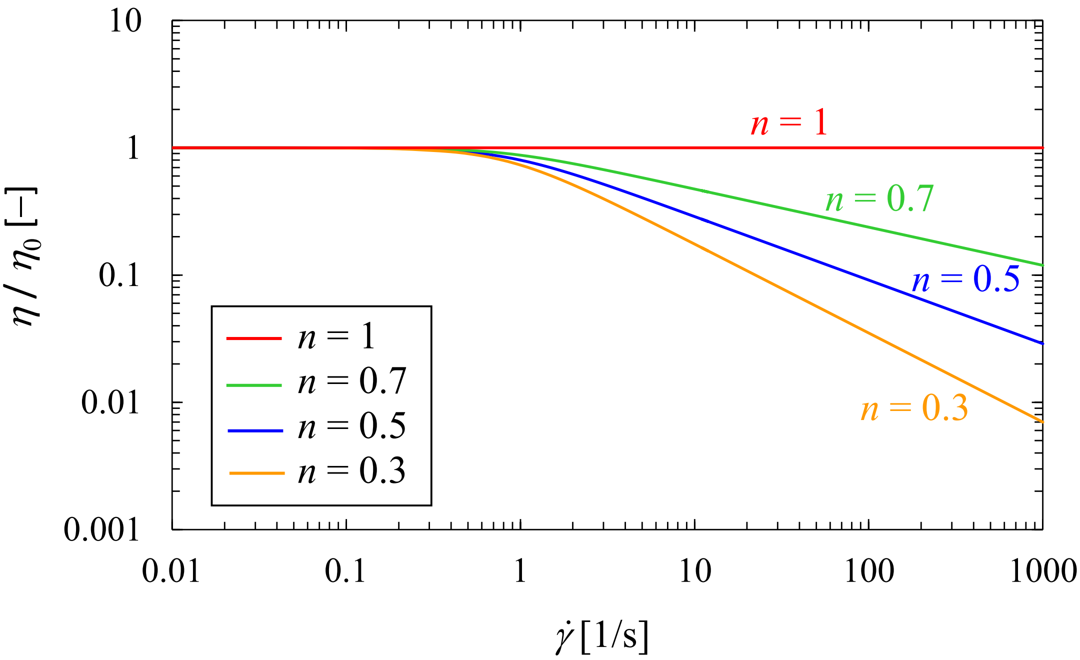

Figure 4 Rheological properties of fluids assumed in this simulation

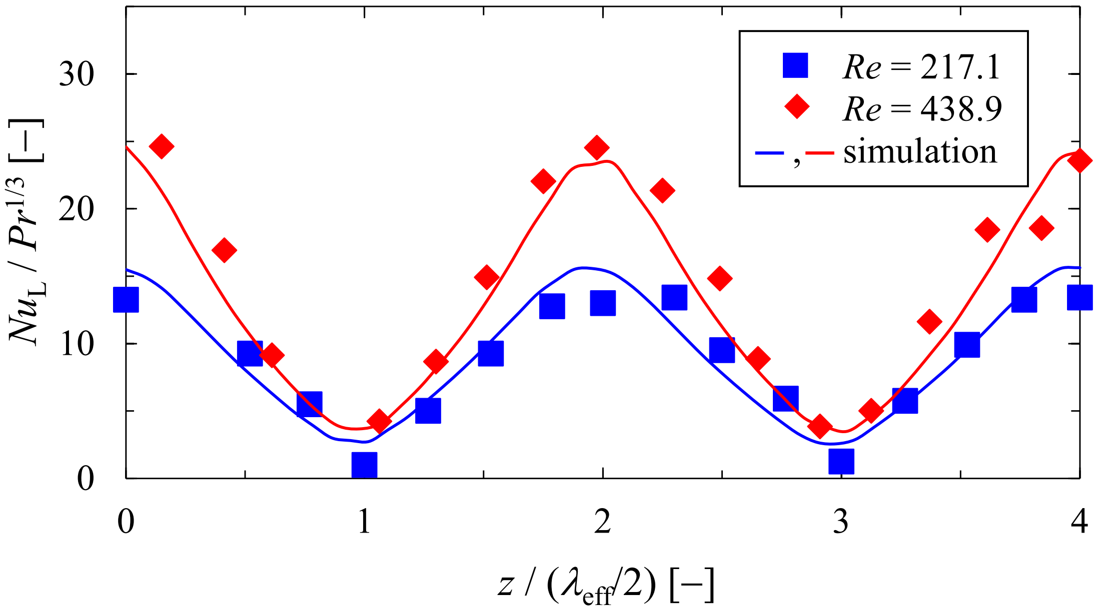

Figure 5 Comparison of simulation results with experiment results

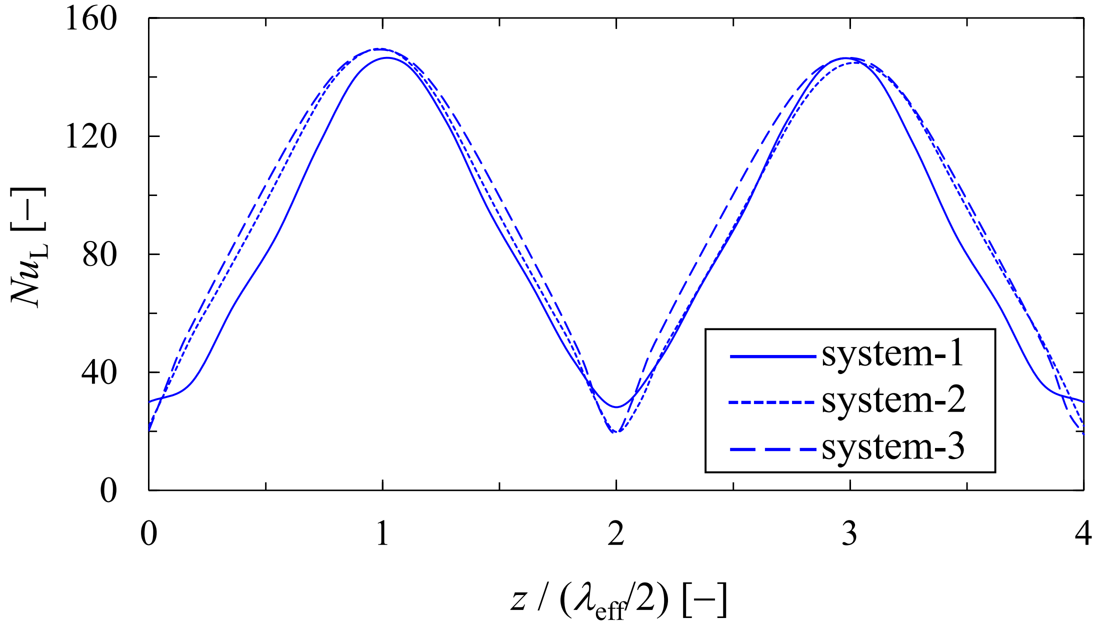

Figure 6 Dependence of simulation results on the mesh number

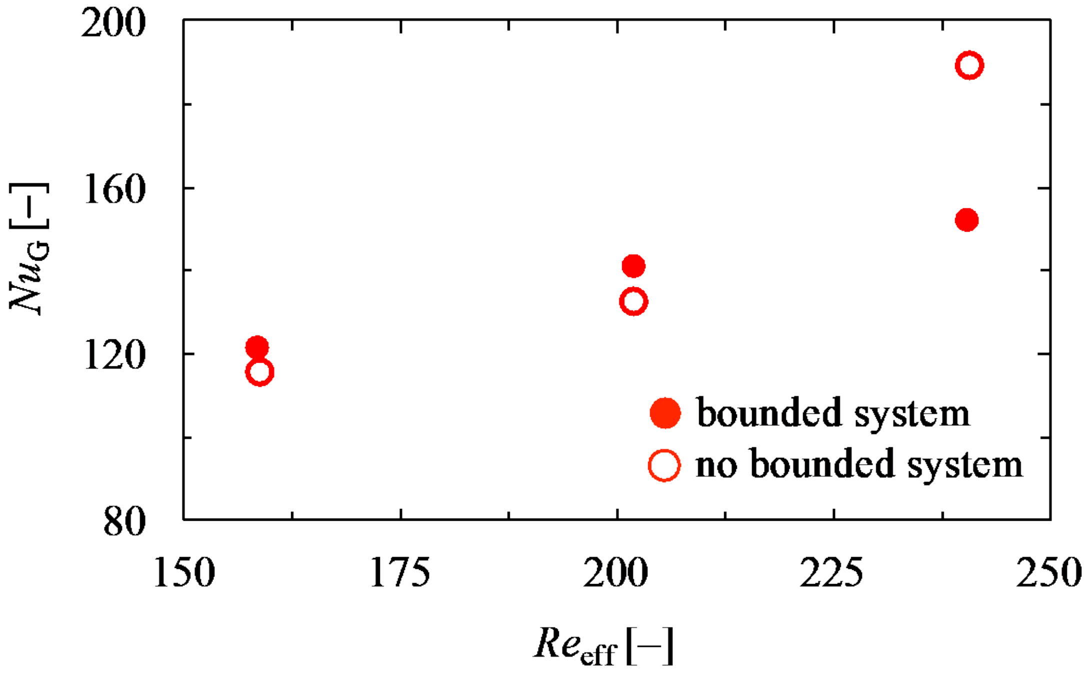

Figure 7 Effect of boundary conditions at side walls on the global Nusselt number (Nu_G)

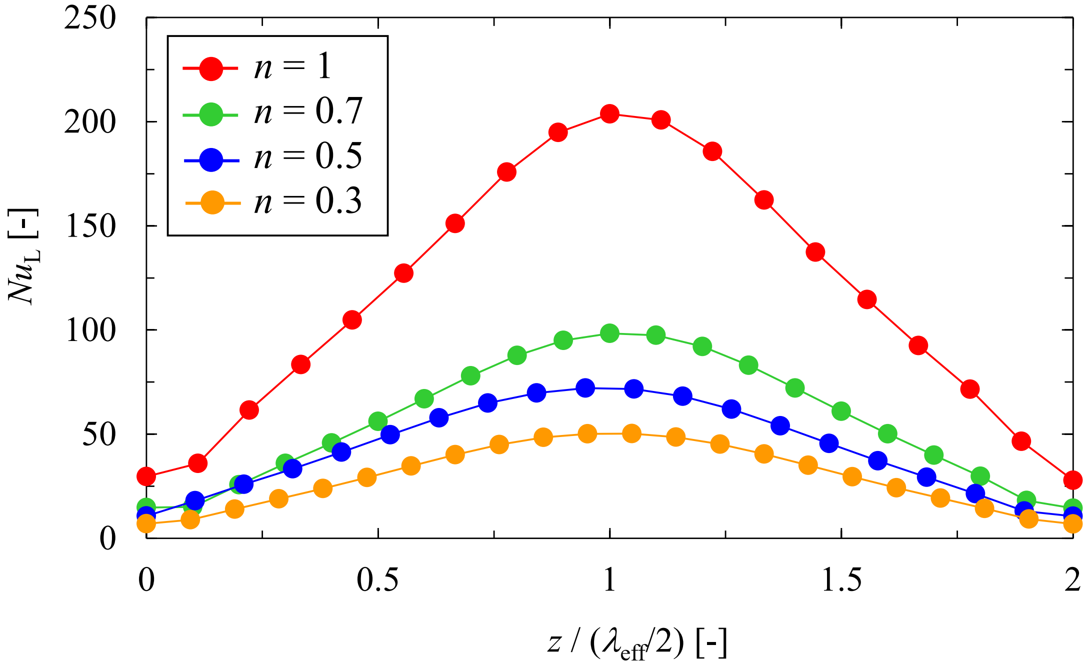

Figure 8 Axial variation in the local Nusselt number (Nu_L) along the surface of the outer cylinder at Re_{eff} = 158

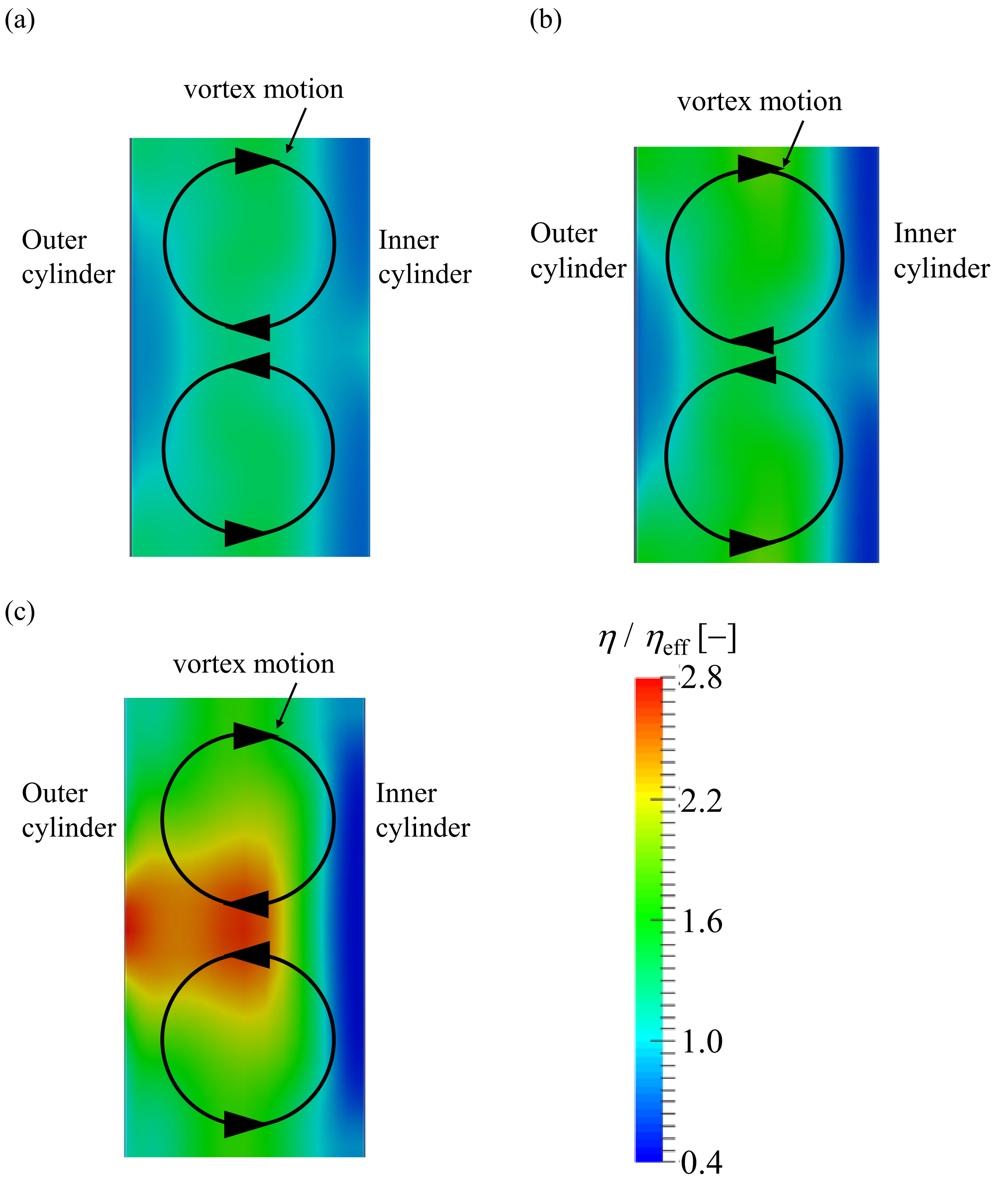

Figure 9 Viscosity distribution in the annular space at Re_{eff} = 158 in the case of (a) n = 0.7, (b) n = 0.5, and (c) n =0.3

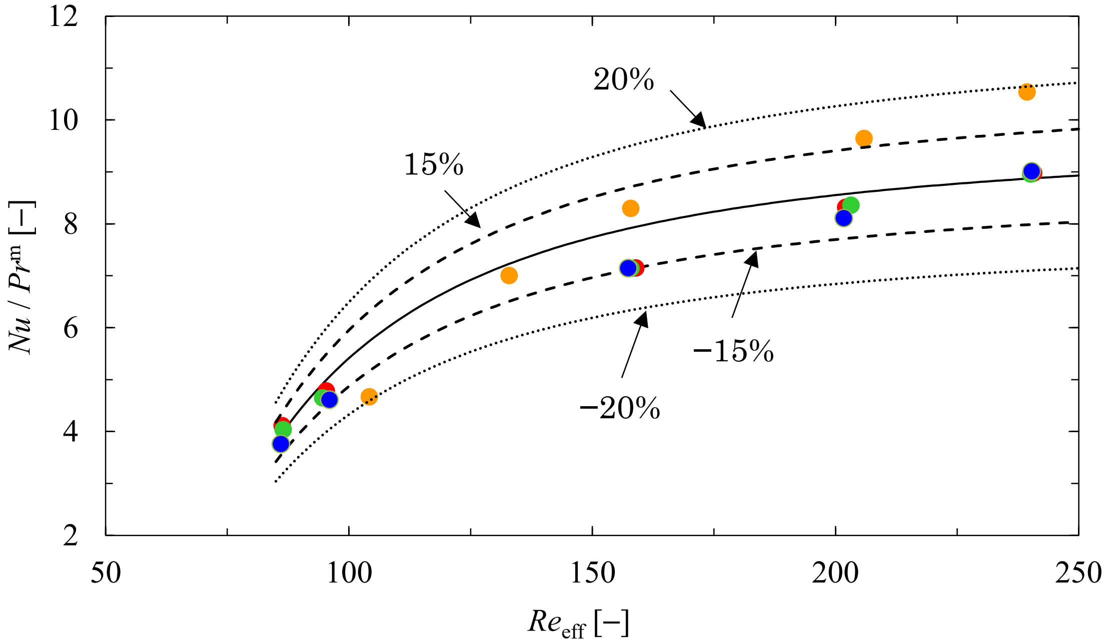

Figure 10 Correlation equation between the global Nusselt number (Nu_G) and Re_{eff}

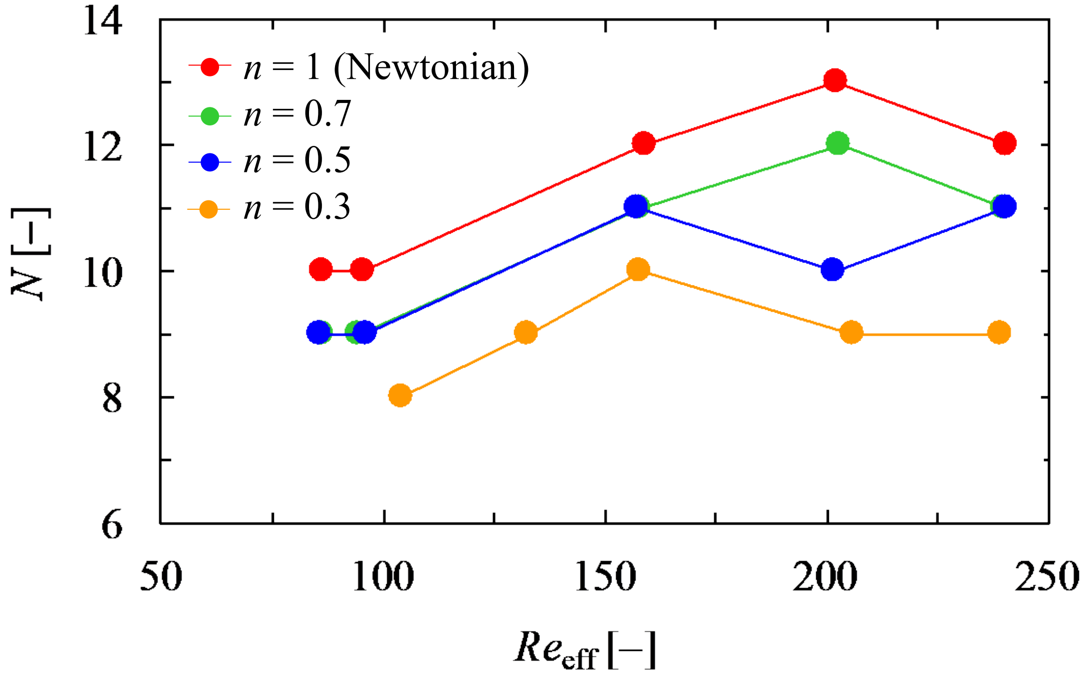

Figure 11 Variation in the number of pairs of Taylor vortices

(a)

(b)

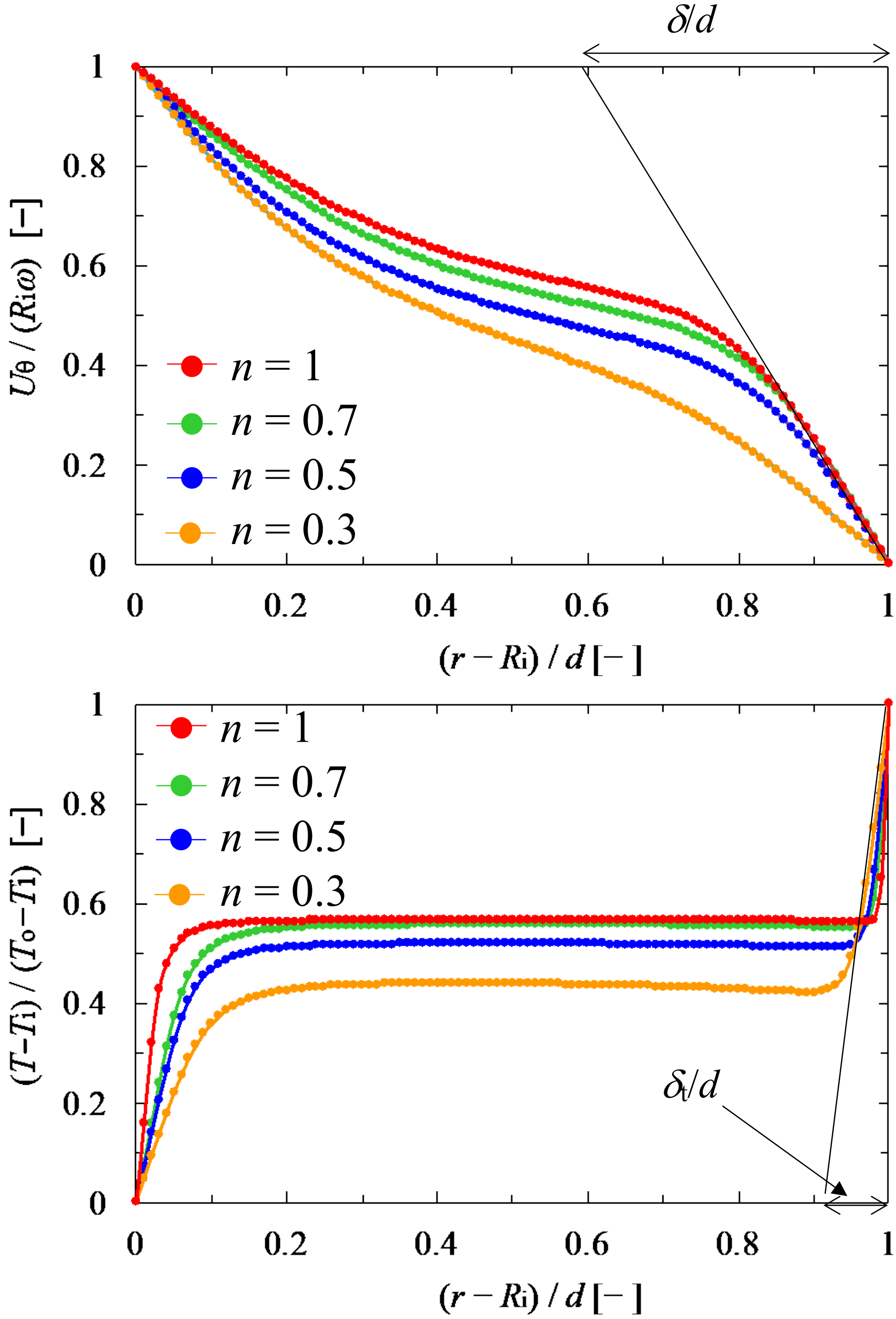

Figure 12 Radial distribution of (a) circumferential velocity and (b) viscosity on the outflow boundary at Re_{eff} = 158

(a)

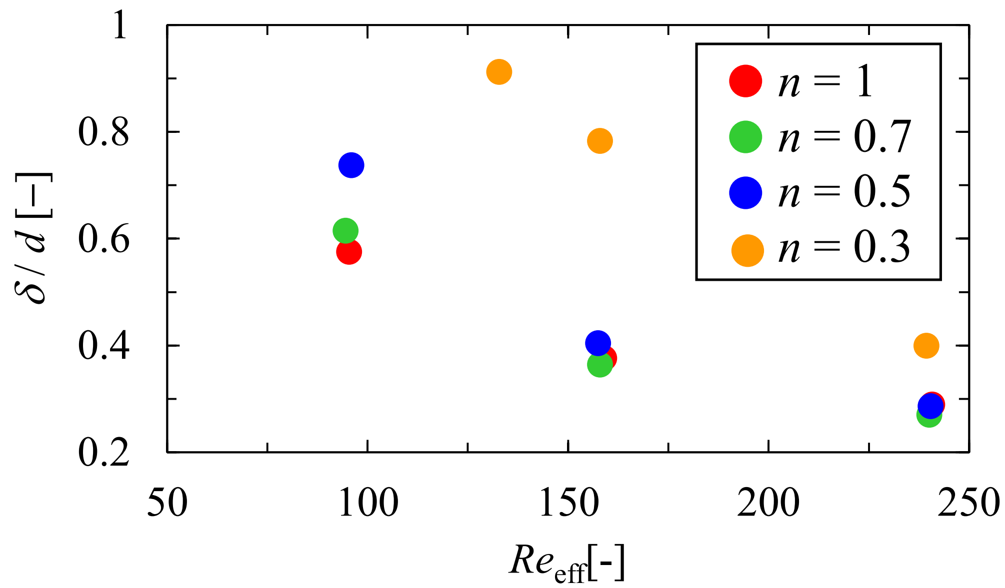

(b)

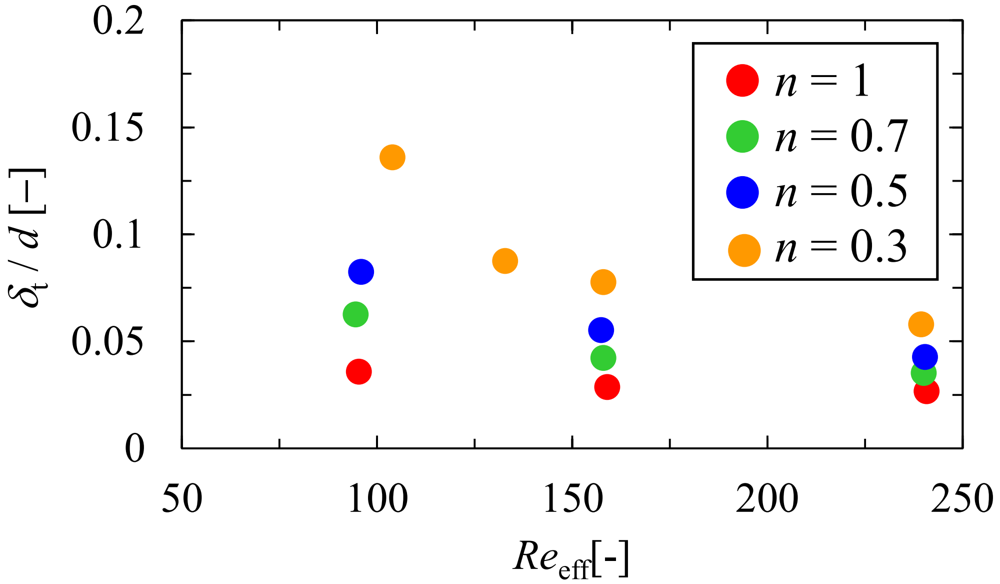

Figure 13Dependence of the dimensionless thickness of (a) the velocity boundary layer and (b) the temperature boundary layer on Re_{eff} at the surface of the outer cylinder on the outflow

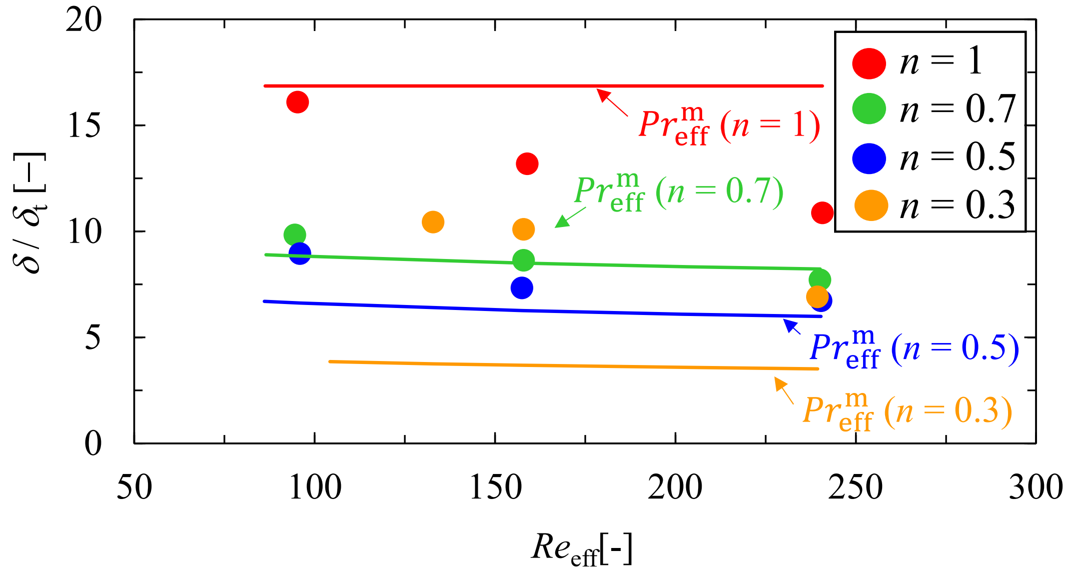

Figure 14 Dependence of ratio of velocity boundary layer thickness on the temperature boundary layer thickness at the surface of the outer cylinder on the outflow, δ/δ_t on Re_{eff}. Solid lines show Pr_{eff}^{m}.